Analytical Biochemistry 632 (2021) 114384

Contents lists available at ScienceDirect

Analytical Biochemistry

journal homepage: www.elsevier.com/locate/yabio

Generation and characterisation of a semi-synthetic siderophore-immunogen conjugate and a derivative recombinant triacetylfusarinine C–specific monoclonal antibody with fungal diagnostic application

Nicola M. Moloney [a,1], Annemarie Larkin [b,2], Linan Xu [a], David A. Fitzpatrick [a], Holly L. Crean [a], Kieran Walshe [a], Hubertus Haas [c], Clemens Decristoforo [d], Sean Doyle [a,*]

[a] Department of Biology, Maynooth University, Maynooth, Co. Kildare, W23 F2H6, Ireland
[b] National Institute for Cellular Biotechnology, Dublin City University, Dublin, Ireland
[c] Institute of Molecular Biology, Medical University Innsbruck, A-6020, Innsbruck, Austria
[d] Department of Nuclear Medicine, Medical University Innsbruck, Anichstrasse 5, A-6020, Innsbruck, Austria

ARTICLE INFO

Keywords:
Siderophore
Immunogen
Hapten
Aspergillus fumigatus
Conjugate vaccine
Competitive ELISA
Lateral flow test
SARS-CoV-2
COVID-19

ABSTRACT

Invasive pulmonary aspergillosis (IPA) is a severe life-threatening condition. Diagnosis of fungal disease in general, and especially that caused by *Aspergillus fumigatus* is problematic. *A. fumigatus* secretes siderophores to acquire iron during infection, which are also essential for virulence. We describe the chemoacetylation of ferrated fusarinine C to diacetylated fusarinine C (DAFC), followed by protein conjugation, which facilitated triacetylfusarinine C (TAFC)-specific monoclonal antibody production with specific recognition of the ferrated form of TAFC. A single monoclonal antibody sequence was ultimately elucidated by a combinatorial strategy involving protein LC-MS/MS, cDNA sequencing and RNAseq. The resultant murine $IgG2_a$ monoclonal antibody was secreted in, and purified from, mammalian cell culture (5 mg) and demonstrated to be highly specific for TAFC detection by competitive ELISA (detection limit: 15 nM) and in a lateral flow test system (detection limit: 3 ng), using gold nanoparticle conjugated- DAFC-bovine serum albumin for competition. Overall, this work reveals for the first time a recombinant TAFC-specific monoclonal antibody with diagnostic potential for IPA diagnosis in traditional and emerging patient groups (e.g., COVID-19) and presents a useful strategy for murine Ig sequence determination, and expression in HEK293 cells, to overcome unexpected limitations associated with aberrant or deficient murine monoclonal antibody production.

1. Introduction

Infection with *Aspergillus* species is termed Aspergillosis and worldwide there are estimated to be over 300,000 cases of life-threatening Aspergillosis in humans per year with mortality rates from 30 to 80% [1–4]. The most devastating manifestation of Aspergillosis is Invasive Pulmonary Aspergillosis (IPA) and this is largely attributed to *Aspergillus fumigatus* [5]. Host status represents the main factor in determining the pathogenicity of *A. fumigatus*. When lung function or the immune system are compromised in some way *A. fumigatus* can effect various forms of disease [5–7]. Lack of early diagnostic methods and limited treatment options are major factors underlying the morbidity of *A. fumigatus* related diseases.

Host status in IPA often contraindicates invasive diagnostic procedures for detection of *A. fumigatus* infection. Two non-invasive diagnostic assays are approved by the US Food and Drug Administration (FDA) utilising cell wall components (galactomannan (GM) and 1,3-β-D-glucan) as biomarkers of *A. fumigatus* infection [8]. 1,3-β-D-glucan is a major component of the fungal cell wall and released from actively growing *A. fumigatus*, but is also found in the cell walls of other fungal species and therefore serves more as a pan-fungal biomarker [9–11]. GM is also found in the fungal cell wall and released from actively growing

* Corresponding author. Department of Biology, Maynooth University, Maynooth, Co. Kildare, Ireland.
E-mail address: sean.doyle@mu.ie (S. Doyle).
[1] Present address: Department of Biochemistry, University of Cambridge, CB2 1QW, United Kingdom.
[2] Present address: Department of Life Sciences, Institute of Technology Sligo, Bellanode, Sligo, F91 YW50, Ireland.

https://doi.org/10.1016/j.ab.2021.114384
Received 19 March 2021; Received in revised form 16 August 2021; Accepted 13 September 2021
Available online 20 September 2021

A. fumigatus in vivo. A monoclonal antibody (mAb) reportedly recognising the side residues of GM was implemented in the Platelia™ assay for the detection of GM in serum or bronchoalveolar lavage (BAL) samples [9]. Though the assay was reported to be quite specific and sensitive, GM is also present in the cell walls of other fungi as well as some drug preparations which can lead to false positives [9]. In 2019 it was revealed that the mAb used in the Platelia™ assay was not specific for GM and that it also recognised other carbohydrate moieties [12]. A lateral flow test (LFT), which uses a mAb (named as JF5 in [13]) to detect an undefined Aspergillus glycoprotein/mannoprotein of approximate molecular mass 40 kDa which is *N*-glycosylated, has also been proposed and validated for diagnosis of IPA (http://olmdiagnostics.com/wp-content/uploads/2018/04/Mar9-AspLFD-A5-SP.pdf). This diagnostic is defined in terms of the mAb used for antigen detection, rather than definition of the precise molecular nature of the fungal antigen upon which diagnosis is made. Together these examples highlight the difficulty associated with identifying biomarkers, and generating diagnostically-useful detection reagents with well-defined antigens, for the specific diagnosis of IA.

During infection, *A. fumigatus* secretes low molecular mass ferric iron (Fe^{3+}) chelators, known as siderophores, that are essential for virulence [14–17]. *A. fumigatus* produces two extracellular siderophores fusarinine C (FsC) and triacetylfusarinine C (TAFC) [18]. Desferri-FsC/TAFC (FsC^{-Fe}/$TAFC^{-Fe}$) chelate extracellular Fe^{3+} and the resulting siderophore-iron complexes (FsC^{+Fe}/$TAFC^{+Fe}$) are taken back up by Siderophore Iron Transporters (SITs) [19,20]. *A. fumigatus* siderophores can also chelate radioactive metals and using this capacity, their utilisation *in vivo* by *A. fumigatus* during infection has been demonstrated [17,21,22]. In addition to directly demonstrating siderophore-mediated iron acquisition *in vivo,* this has been an innovative means of imaging *A. fumigatus* infection thereby providing a non-invasive *in vivo* diagnostic strategy, albeit requiring expensive equipment and significant expertise [23]. Siderophores can also be used to address the current deficit in non-invasive *A. fumigatus* infection diagnostics whereby detection of siderophores in biological samples (such as urine, BAL, or serum) from patients acts as a biomarker of infection [24]. Detection of *A. fumigatus* siderophores in mammalian host samples has been demonstrated to have diagnostic utility using LC-MS/MS, CE-ESI-MS and HPLC analyses [23,25–28].

While the above work provides evidence for the use of siderophores as biomarkers for *A. fumigatus* infection with highly sensitive detection systems, these are costly procedures, requiring appropriate facilities and highly trained operators. Immunoassays or point-of-care assays offering rapid results, lower associated cost and relatively easier use have potential for wider implementation. Antibodies form the basis of many such assays, for example in the GM assay. The prerequisite for this strategy is the generation of mAbs directed against the small target molecule, and the subsequent use of those novel antibodies to detect the small molecule, produced by the infectious agent, at high sensitivity and specificity. To address this, here we describe the preparation of a semi-synthetic siderophore immunogen for the generation of an *anti*-TAFC IgG, the sequence of which was determined using a proteo-transcriptomic approach so that it could recombinantly expressed and used for the development of TAFC-specific ELISA and LFT detection systems.

2. Materials and methods

2.1. Immunogen synthesis strategy for generating TAFC antibodies

An analog strategy was used to develop a TAFC immunogen whereby conjugation of the TAFC analog (diacetylated fusarinine C; DAFC) to the carrier protein, keyhole limpet haemocyanin (KLH), was mediated by heterobifunctional crosslinkers, sulphosuccinimidyl-4-(*N*-maleimidomethyl)cyclohexane-1-carboxylate (sulpho-SMCC) and *N*-succinimidyl *S*-acetylthioacetate (SATA), respectively [29,30]. Importantly, TAFC generated by sulphosuccinimidyl NHS-acetate (SNA)-mediated acetylation shares an LC-MS/MS retention time and fragmentation pattern with that of native TAFC acetylated by the *A. fumigatus* acetyltransferase, SidG, confirming that it is suitable for generation of an acetylated TAFC analog (Supplementary Fig. 1). The strategy for generating the TAFC immunogen is summarised in Fig. 1. In detail, ferrated FsC (FsC^{+Fe}) was obtained from *A. fumigatus* iron-free culture supernatants via Sep-Pak C_{18} concentration and RP-HPLC purified (5.8 mM FsC^{+Fe} in 50 mM sodium phosphate pH 7.2) [30]. FsC^{+Fe} was acetylated via sequential addition of SNA with RP-HPLC monitoring until maximal DAFC levels were obtained. The acetylated FsC^{+Fe} reaction mixture was brought to 5.6 mM total siderophore for sulpho-SMCC derivatisation, whereby 13.4 μmol sulpho-SMCC (268 μL; 50 mM in DMSO) was added to 15.1 μmol of the acetylated FsC^{+Fe} reaction (2.7 mL; 5.6 mM). The reaction was agitated gently at room temperature in the dark for 1 h. Deblocked SATA-KLH [29] containing 166 nmol –SH (2.8 mg mL^{-1}; 2.3 mL in KLH conjugation buffer) was added to 15 μmol of acetylated FsC^{+Fe}-SMCC reaction (2.95 mL; 5.1 mM FsC^{+Fe} 4.4 mM sulfo-SMCC). The reaction was incubated at room temperature in the dark for 30 min followed by rotating at 4 °C overnight. After conjugation the reaction mixture which should contain DAFC-KLH, was dialysed against PBS, the siderophore content estimated at 440 nm and protein content measured by Bradford. SATA-BSA was similarly modified with DAFC to yield DAFC-BSA.

2.2. Generation of TAFC IgG antibody

The acetylated FsC-KLH immunogen (DAFC-KLH; 50 μg combined soluble and insoluble) was mixed with adjuvant, Pam3Cys-SKKK (EMC Micro collections, Germany) in a final volume of 100 μL and intraperitoneally administered to BALB/c mice ($n = 3$; 6–8 weeks old). Immunisations were carried out at the Royal College of Surgeons (RCSI) Biomedical Research Facility, Beaumont Hospital, Dublin 9, Ireland; all immunisation protocols were licensed (Licence number: B100/3676) by the Department of Health and Children, Ireland. Mice received three additional boosters of the same composition over 3-week intervals. After the third booster, tail bleeds were taken and sera isolated for polyclonal antibody analysis [31]. Sera were screened for polyclonal antibodies with specificity for TAFC, and also against unrelated metabolites or ions including free iron and bis(methylthio)gliotoxin (BmGT) [32]. Tail bleed serum was diluted 1 in 80,000 and analysed by competitive ELISA ($n = 2$) with a DAFC-BSA coating concentration of 0.12 μg mL^{-1} in 50 mM sodium carbonate pH 9.6. After immunisations and tail bleed analysis, a single mouse was selected for the development of *anti*-TAFC IgG producing hybridoma cells. A fourth and final booster of the DAFC-KLH immunogen (50 μg) was mixed with Pam3Cys-SKKK in a final volume of 100 μL and intraperitoneally administered to BALB/c mice 3 days prior to the fusion. Cell fusion of the immunised spleen B-cells with SP/2/O–Ag myeloma cells was carried out using a modification of the fusion protocol outlined in [33]. Fused cells were plated out in 48-well plates containing HAT selection medium and 5% (v/v) Briclone (NICB, DCU, Ireland) and incubated undisturbed for 10–12 days in a humidified chamber at 37 °C/5% CO_2. Hybridoma culture supernatant was screened by competitive ELISA ($n = 1$) with the same conditions as for the antisera screening with and without competing TAFC (100 μM only). Positively identified hybridomas from this screen were sub-cultured and supernatant screened again by competitive ELISA ($n = 1$). Isotype of selected hybridomas was determined using the Isostrip™ Mouse Monoclonal Antibody Isotyping Kit (Roche). After process optimisation, *anti*-TAFC IgG was purified from the selected hybridoma cell line (named 6C6) by Protein A affinity chromatography and subjected to immunoaffinity analysis and purification using DAFC-sensitised paramagnetic beads.

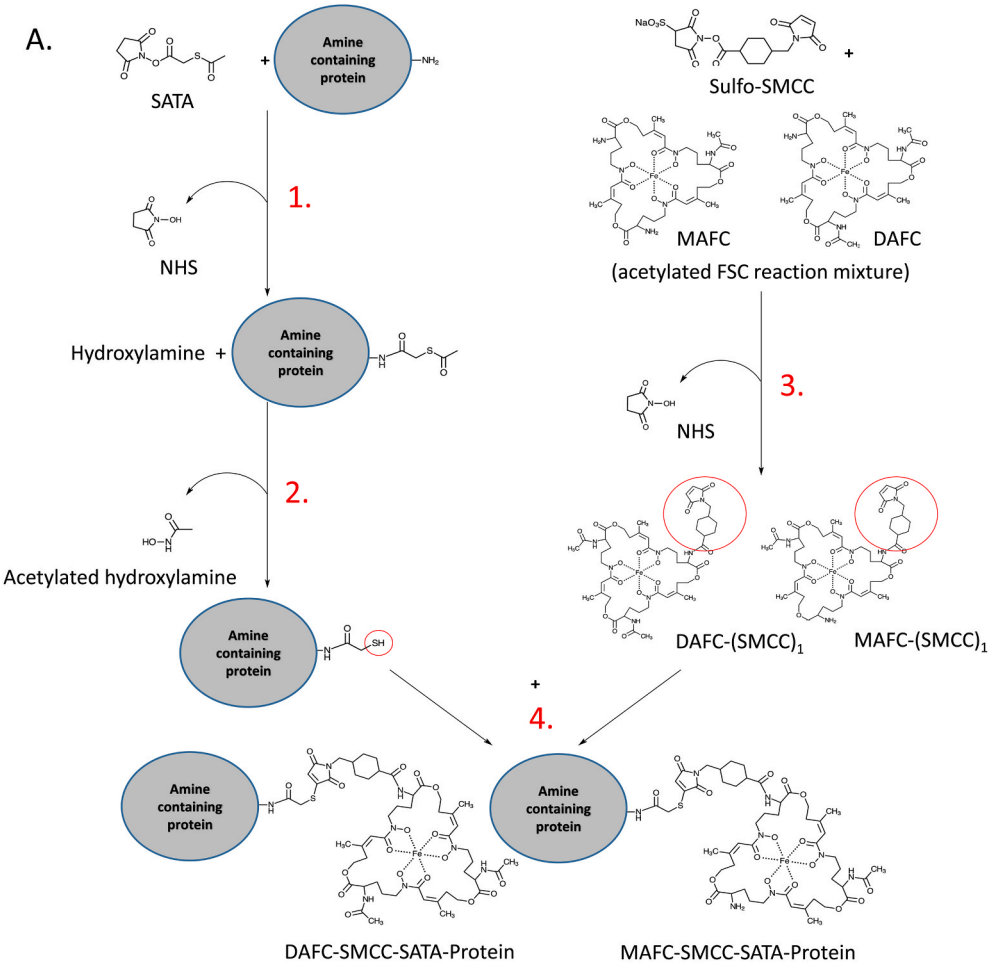

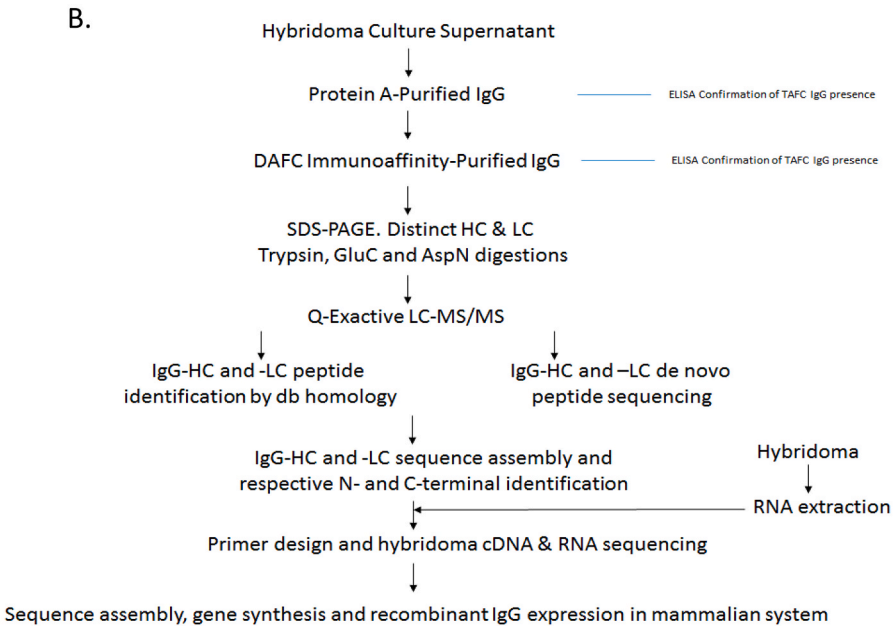

Fig. 1. A. Strategy for the development of a semi-synthetic TAFC immunogen. 1. KLH was modified with SATA via NHS ester linkage to amine groups, introducing protected thiol groups. 2. Thiol groups of SATA-KLH were deprotected by hydroxylamine. Excess SATA and hydroxylamine are removed by gel filtration. 3. Acetylated FsC was modified with sulpho-SMCC to introduce a thiol-reactive maleimide group and generate MAFC-$(SMCC)_1$ and DAFC-$(SMCC)_1$. 4. When combined, the thiol group of SATA-KLH could form a stable thioether bond with the maleimide group of MAFC-SMCC or DAFC-SMCC. Excess unconjugated siderophore and crosslinker were removed by dialysis prior to murine immunisation. B. Overview of the strategy used to isolate, sequence and express the TAFC monoclonal antibody produced by the unstable and impure hybridoma population.

2.3. Coating of paramagnetic beads with DAFC and immunoaffinity purification of IgG

Acetylated FsC^{+Fe} was prepared similarly to that described for the immunogen synthesis, however the FsC^{+Fe} was not RP-HPLC purified and acetylation was carried out in 0.1 M $NaHCO_3$ pH 8.5, followed by organic extraction with chloroform. *N*-hydroxysuccinimide-activated paramagnetic beads (300 μL; Pierce™) were equilibrated to room temperature and washed with ice-cold 1 mM HCl (1 mL). The acetylated FsC^{+Fe} (300 μL; 5.2 mM siderophore in 0.1 M $NaHCO_3$) was added to beads followed by incubation for 2 h while rotating at room temperature, with periodic vortexing. Beads were washed extensively and stored following manufacturer instructions. For immunoaffinity purification beads were incubated with blocking solution (1% BSA in Tris Buffered Saline-Tween (TBST)) for 15 min at room temperature. Protein A-purified *anti*-TAFC IgG (4 mL at 0.3 mg mL^{-1} in TBST) was added to beads followed by incubation for 2 h at room temperature while rotating. After extensive TBST washing, *anti*-TAFC IgG was eluted in 0.1 M glycine pH 2 followed by neutralisation with 1 M Tris pH 9 and analysed by absorbance at 280 nm, ELISA and SDS-PAGE.

2.4. LC-MS/MS analysis of affinity and immunoaffinity-purified TAFC IgG

To obtain the complete sequence of the *anti*-TAFC IgG (Fig. 1B), initially a solely proteomic strategy was implemented whereby LC-MS/MS was utilised in an attempt to derive the full sequence associated with the immunoaffinity purified *anti*-TAFC IgG. Firstly, Protein A and immunoaffinity-purified TAFC IgG were subjected to SDS-PAGE [29]. All observed heavy and light chain bands were excised in three pieces each and digested with trypsin, Asp-N, or Glu-C [34]. An in-solution digestion with trypsin, Asp-N, or Glu-C of immunoaffinity purified IgG was also carried out in parallel. All peptides were analysed by Q-Exactive LC-MS/MS [35,36]. Mass spectra from the analysis of antibody heavy and light chains before and after immunoaffinity purification (following in-gel digestion) were analysed using PEAKS Studio (version 8.0) following the ALPS pipeline developed for peptide identification and protein sequence assembly using the associated assembler tool [37]. Briefly, raw files for the same band digested with three different enzymes were imported together and treated as a single sample. Generally, an error tolerance of 10 ppm and 0.02 Da was permitted for the precursor and fragmentations, respectively. Modifications included: carbamidomethylation (fixed), oxidation of methionines (variable), and deamidation of asparagine/glutamine (variable). At most, three modifications were permitted per peptide. Local confidence scores of peptides identified by *de novo* sequencing were accepted if above 50%. For database searching, initially a database of murine antibody sequences (from [37]) was used. Following isotyping, a modified database supplemented with additional murine IgG_{2a} κ antibody sequences from the online database, abYsis (www.abysis.org) was used [38]. Three lists of peptides were generated for each sample corresponding to: (i) *de novo* sequencing results, (ii) standard database search results paired with remaining unmatched over *de novo* sequencing results, (iii) SPIDER database search results paired with remaining unmatched over *de novo* sequencing results. After exporting peptide lists, determination of the full-length antibody sequence was attempted using all identified peptides with the ALPS assembler tool. Peptides generated from the assembler and peptides manually extracted from database matches were collected, refined to reduce redundancy and remove contaminants. Putative sequences were derived by aligning the sequences with several template antibody sequences. Alignments were visualised using Clustal Omega or MUSCLE in R using bioconductor package, msa or online.

2.5. RNA isolation and RNAseq analysis of 6C6 hybridoma RNA

cDNA was obtained by use of TRIzol reagent (Thermo Fisher Scientific) to isolate hybridoma RNA, followed by cDNA synthesis using cDNA synthesis kit (Thermo Fisher Scientific). Total 6C6 hybridoma RNA was isolated using Trizol reagent according to the manufacturer's instructions. Following analysis using an Agilent 2100 Bioanalyzer, this material consisted of high quality RNA and exhibited a RIN value = 8.4 and 28S/18S = 1.2, and was then subjected to Illumina sequencing using an Illumina HiSeq™4000 (BGI, Hong Kong, China).

2.6. Bioinformatic pipeline for RNAseq interrogation and TAFC-specific IgG production

Reads were first trimmed and low quality reads were removed using Trimmomatic [39]. Overall sequencing quality was extremely high as assessed using FASTQC (http://www.bioinformatics.babraham.ac.uk/projects/fastqc/). Total reads were *de novo* assembled using Trinity [40]. We used igfinder [41] to extract the *Igh* and *Igl/Igk* CDSs by retaining contigs that contained 20–30 bp of unique sequences of the *Igh* and *Igl/Igk* constant region and were of appropriate length (*Igh* > 1200 bp, *Igl/Igk* > 600 bp). Constituent IgG nucleotide sequences from RNAseq analysis ($n = 43$) were translated into the three possible reading frames (using the standard genetic code with http://www.bioinformatics.org/sms2/translate.html) to generate a list of translated amino acid sequences ($n = 129$) [42]. The resultant sequences were appended to the previous database comprised of sequences of murine antibodies from [37], additional antibody sequences (IgG_{2a} and κ antibody chains) from abYsis (www.abysis.org) and common contaminants. Mass spectra from the analysis of antibody heavy and light chains before and after *anti*-TAFC IgG immunoaffinity purification (following both in-gel and in-solution digestion) were searched against this database using MaxQuant (v1.6.1.0). Samples were analysed according to the enzyme used for protein digestion and spectra of the same protein digested with the three enzymes were grouped together. Search parameters were as above. After MaxQuant analysis, protein groups were exported and processed in Perseus (v1.5.5.0) for data filtering. Once a sequence had been identified, the *anti*-TAFC recombinant antibody was produced by commercial arrangement (Genscript) by transient infection of a HEK293 cell line, secretion, purification and storage at −25 °C until required.

2.7. TAFC competitive ELISA

For analysis of murine antisera, hybridoma culture supernatant and Protein-A or immunoaffinity purified hybridoma-produced IgG, competitors (50 μL) were added to DAFC-BSA-coated (0.12 μg mL^{-1}) ELISA plate wells immediately before addition of antibody (50 μL). For recombinantly produced *anti*-TAFC IgG, IgG (3 ng mL^{-1}) was co-incubated with TAFC standards (0–1 μM TAFC) for 30 min at room temperature prior to addition (100 μL/well, in duplicate) to DAFC-BSA-coated (0.12 μg mL^{-1}) ELISA plate wells. After 60 min incubation at 37 °C, wells were washed with PBST (300 μL/well; 4x) followed by anti-mouse IgG-HRP conjugate addition (100 μL/well) for 40–60 min at 37 °C. Wells were again washed with PBST followed by the addition of Teramethylbenzidine substrate (100 μL; Moss Inc) for 10 min and Stop solution (100 μL/well; 1 N sulphuric acid) and absorbance determined at 450/620 nm.

2.8. Single-pot DAFC-BSA preparation for lateral flow test

Sulpho-SMCC (28 μL; 6.4 mg 300 μL^{-1} dimethylformamide (DMF)) was added to 150 μL FsC^{+Fe} (1.1 mg 150 μL^{-1} PBS- 1 mM EDTA pH 7.8), mixed by brief vortexing and incubated at room temperature (RT) for 1 h. SNA (10 μL; 1.4 mg 20 μL^{-1} DMF) was then added to the FsC^{+Fe}/sulpho-SMCC reaction mixture and incubated at RT for a further 1 h. Simultaneously with FsC^{+Fe} activation, 0.5 mL 0.5 M hydroxylamine was added to 5 mL SATA-BSA (1 mg mL^{-1} in PBS-1 mM EDTA pH 6.8) [29], mixed gently and incubated at RT for 1 h to expose thiols. Then the SNA/FsC^{+Fe}/sulpho-SMCC reaction mixture was added to the treated

SATA-BSA, mixed to ensure homogeneity and incubated at RT for 2 h, and then 4 °C overnight, with gentle shaking. After conjugation was completed, 2 x 50 μL 100 mM *N*-ethylmaleimide, was added to the conjugation mixture for 20 min to deactivate any residual free thiol groups. The conjugate was then dialysed versus PBS- 1 mM EDTA, 2 x 50 vol, 3 h each, stirring 4 °C and stored at −20 °C.

2.9. DAFC-BSA conjugation to AuNP and lateral flow test development

DAFC-BSA (10 mL; 20 μg mL^{-1}) was prepared in 2 mM sodium borate pH 8.0 and added to 10 ml AuNP (20 nm diameter) mixed rapidly, followed by incubation at RT for 30 min with rotating. BSA (10%(w/v); 1 mL in 25 mM sodium borate pH 8.0) was then added to stabilize the conjugate, and incubated for 30 min with rotating followed by centrifugation at 3600 g for 30 min. The pellet was collected and resuspended in 1 mL 1%(w/v) BSA in 25 mM sodium borate pH 8.0, and the A_{520nm} determined. This reagent was termed DAFC-AuNP conjugate. 40 μL 1%(w/v) NaN_3 was added to the resuspended pellet and the supernatant and mixed gently. TAFC-specific IgG (300 μg mL^{-1} in PBS) was sprayed onto test membranes (Millipore Hi-Flow plus 180 membrane cards 60 mm × 301 mm) using an Isoflow™ Dispenser at a rate of 0.10 μL mm^{-1}. Membranes were air dried for 30 min, sample and wicking pads applied, and then cut into 4.20 mm width strips using a Kinematic Automation Matrix 2360 cutter. Buffer (0.05%(v/v) Tween-20 in PBS), DAFC-AuNP conjugate (10–100 μL) and TAFC at various concentrations were added to a final volume of 200 μL in microwells, to which test strips were then placed and test strips allowed to develop for 30 min.

3. Results

3.1. Conjugation of acetylated FsC^{+Fe}-SMCC to SATA-KLH

Activation of acetylated FsC^{+Fe} with sulpho-SMCC was demonstrated whereby generation of mono(M)AFC-$(SMCC)_1$ and DAFC-$(SMCC)_1$ were confirmed by LC-MS/MS and RP-HPLC analysis (Fig. 2A–D and Supplementary Fig. 2). FsC^{+Fe} was RP-HPLC purified and acetylated via sequential addition of SNA. This was analysed by RP-HPLC to estimate relative levels of FsC, MAFC, DAFC, and TAFC (Supplementary Fig. 2). Subsequently, the acetylated FsC was derivatised by the addition of sulpho-SMCC equimolar to the relative moles of FsC, MAFC, and DAFC. An aliquot of the reaction was quenched and analysed by RP-HPLC, which indicated that 14% and 10% of the total siderophore was converted to MAFC-$(SMCC)_1$ and DAFC-$(SMCC)_1$, respectively (Supplementary Fig. 2). The acetylated FsC-SMCC reaction mixture was immediately added to demasked SATA-KLH with at least 10X molar excess of MAFC-$(SMCC)_1$ and DAFC-$(SMCC)_1$ to total thiol groups. For comparative analytical purposes, a small scale of the sample and a negative control (using acetylated FsC^{+Fe} without sulpho-SMCC modification) were conducted in parallel. Following the conjugation reaction, the small-scale sample and negative control were purified by PD10 separation and the OD_{440} of each protein-containing fraction was measured to determine the OD_{440} mg^{-1} protein. Protein-containing fractions from the small-scale sample showed an average OD_{440} of 0.22 mg^{-1} protein while the negative control showed an OD_{440} of 0.09 mg^{-1} protein (Supplementary Fig. 2). This indicated successful conjugation, whereby without sulpho-SMCC in the reaction, free unconjugated siderophore was removed following size exclusion separation. The OD_{440} and Bradford assay were used to determine the siderophore and protein content to be 181 μM and 1.4 mg mL^{-1} respectively, confirming conjugation of 129 nmol siderophore mg^{-1} KLH.

3.2. Anti-TAFC specific polyclonal antibodies are present in mouse sera

ELISA analysis indicated the presence of competitive *anti*-TAFC antibodies in DAFC-KLH-immunised murine serum with no competition for free iron or BmGT at the same concentration (Fig. 3A). This indicates that the polyclonal antibodies were specific for TAFC. A pre-immunisation serum taken from one of three mice prior to DAFC-KLH immunisation was also diluted 1 in 100,000, analysed by ELISA and showed no binding to DAFC-BSA ELISA plates (Fig. 3A).

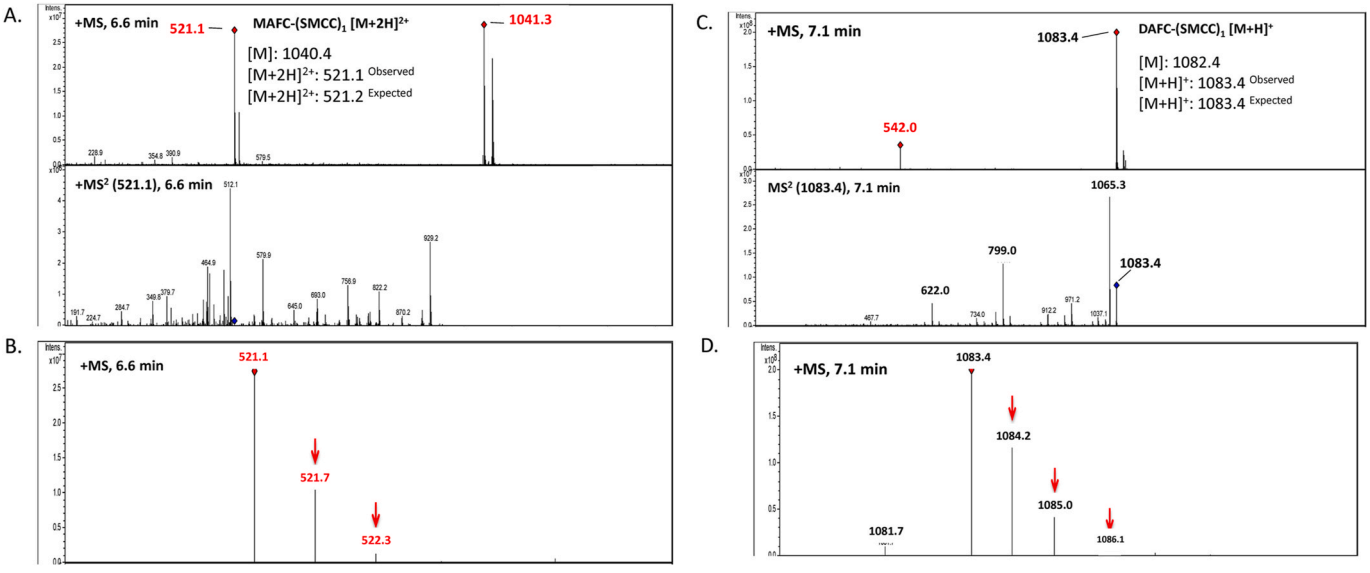

Fig. 2. LC-MS/MS identification of MAFC-$(SMCC)_1$. A. Peak associated with MAFC-$(SMCC)_1$ (peak 5. in Supplementary Fig. 2) was analysed by LC-MS/MS. MS (extracted ion chromatogram for *m/z* 518–524) spectrum shows the detection of MAFC-$(SMCC)_1$ as a doubly charged ion (M: 1040.4, $[M+2H]^{2+}$: observed *m/z* 521.1; expected *m/z* 521.2). MS2 spectrum shows the fragmentation of precursor ion. B. Increments of approx. +0.5 in observed *m/z* are indicative of C_{13} isotope incorporation in a doubly charged ion. C. LC-MS/MS identification of DAFC-$(SMCC)_1$. Peak associated with DAFC-$(SMCC)_1$ (peak 6. in Supplementary Fig. 2) was analysed by LC-MS/MS. MS (extracted ion chromatogram for *m/z* 1081–1085) spectrum shows the detection of DAFC-$(SMCC)_1$ as a singly charged ion (M: 1082.4, $[M+H]^{+}$: observed *m/z* 1083.4; expected *m/z* 1083.4). MS2 spectrum shows the fragmentation of precursor ion. D. Increments of approximately +1.0 in observed *m/z* are indicative of C_{13} isotope incorporation in a singly charged ion.

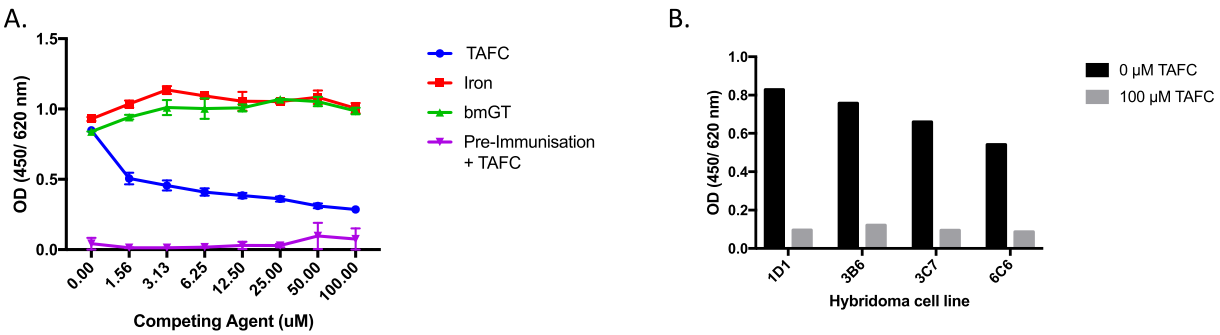

Fig. 3. A. Competitive ELISA analysis to establish specificity of *anti*-TAFC polyclonal antibodies. Tail bleeds from the selected mouse were analysed by competitive ELISA with competitors; TAFC, iron, and BmGT. Only addition of competing TAFC resulted in a decreased OD (450/620 nm) with increasing competitor concentration. Pre-immunisation serum was also analysed and showed no affinity for DAFC-BSA coated ELISA plates. B. Indirect competitive ELISA screening of candidate hybridomas; 1D1, 3B6, 3C7, and 6C6. Hybridoma supernatant was screened by competitive TAFC ELISA, by addition to ELISA plates wells with and without 100 µM TAFC. Cells which produced IgG with affinity for plate coated DAFC-BSA that showed inhibition upon the addition of competing TAFC were regarded as positive and moved to 6 well plates. All hybridoma supernatants showed some degree of competition for free TAFC.

3.3. Generation of hybridoma cells producing anti-TAFC antibodies and screening of hybridoma cells following fusion

Following the fusion of the splenocytes from the selected mouse with SP/2/O–Ag 14 myeloma cells, a 66.2% fusion efficiency was observed with 247 out of 342 wells on 48 well plates showing hybridoma development. Hybridoma supernatant containing putative IgG with affinity for microwell-immobilised DAFC-BSA, that showed reduced binding upon addition of competing ferrated TAFC ($TAFC^{+Fe}$), were regarded as positive. In total, hybridoma supernatants from 74 wells were screened this way and 26 of these were transferred to 6 well plates for further sub-culturing, screening and cryopreservation. Fig. 3B shows

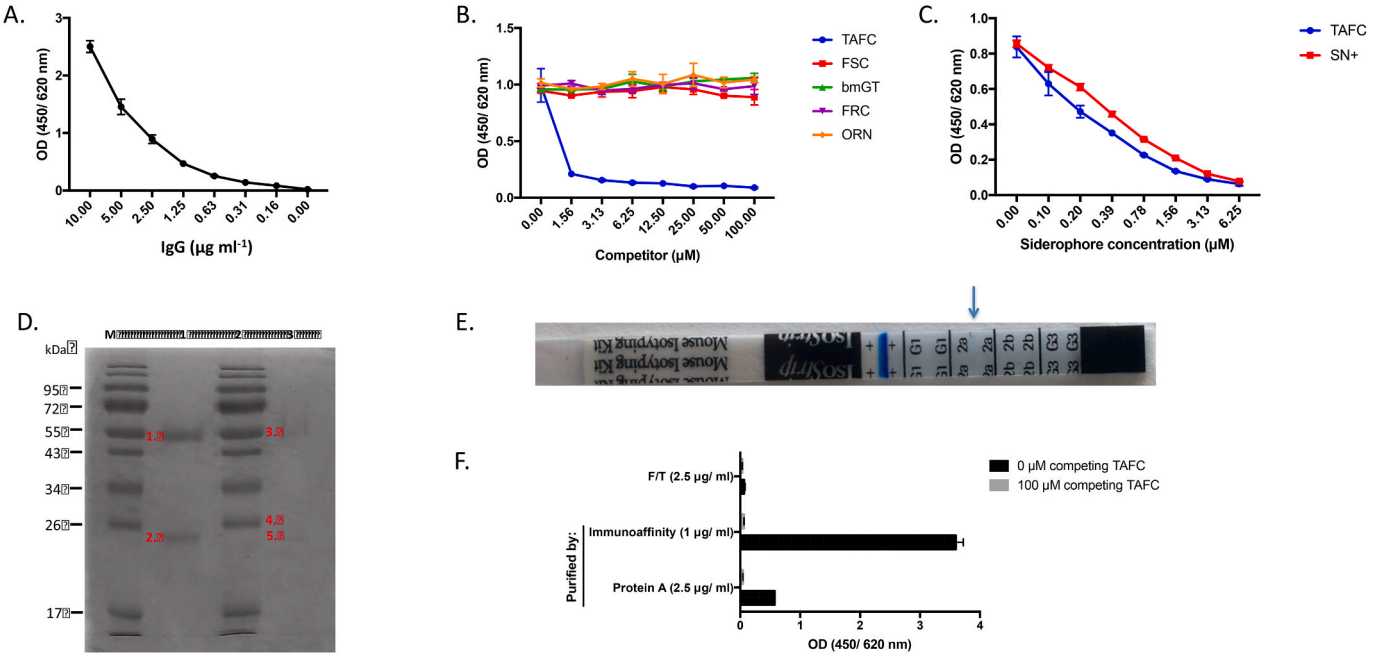

Fig. 4. A. Optimisation of IgG concentration (µg mL^{-1}) for ELISA analysis. IgG was titred (0.16–10 µg mL^{-1}) and added to DAFC-BSA coated ELISA plates to determine the optimal concentration of IgG to use for further ELISA analysis. An IgG concentration of 2.5 µg mL^{-1} was selected for further ELISA analysis. B. Competitive ELISA analysis of *anti*-TAFC IgG indicates high specificity for TAFC. Purified IgG was analysed by competitive ELISA with a titre (1.56–100 µM) of several competitors; ferri-triacetylfusarinine C (TAFC), ferri-fusarinine C (FsC), bis(methylthio)gliotoxin (BmGT), ferrichrome (FRC), and ferri-ornibactin (ORN) on acetylated FsC-BSA coated ELISA plates. IgG shows competition with TAFC (mean $OD_{450/620}$ 0.99 at 0 µM TAFC and 0.09 at 100 µM TAFC), but not other metabolites. C. Competitive TAFC ELISA analysis of purified *anti*-TAFC IgG. IgG purified from 6C6 culture supernatant was analysed by competitive TAFC ELISA using TAFC and ferrated wild-type supernatant (SN+). IgG showed decreasing OD (450/620 nm) with increasing competing TAFC concentration from (i) TAFC (mean $OD_{450/620}$ 0.84 at 0 µM TAFC and 0.06 at 6.25 µM TAFC) and (ii) SN+ (mean $OD_{450/620}$ 0.86 at 0 µM TAFC and 0.08 at 6.25 µM TAFC). D. SDS-PAGE analysis of *anti*-TAFC IgG before and after immunoaffinity purification loaded with: M: Molecular mass marker. 1: Protein A-purified IgG. 2: Molecular mass marker. 3. Anti-TAFC immunoaffinity purified IgG. Numbers indicated position of 1. Heavy chain before immunoaffinity purification, 2. Light chain before immunoaffinity purification, 3. Heavy chain after immunoaffinity purification, 4. Light chain A (LCA) after immunoaffinity purification and 5. Light chain B (LCB) after immunoaffinity purification. These numbers correspond to identifiers used in MaxQuant analysis in Supplementary Table 6. The higher light chain band present after immunoaffinity purification (light chain A) was not visible after scanning. E. Isostrip™ analysis of immunoaffinity-purified TAFC IgG indicated it produced an IgG_{2a} heavy chain and kappa light chain. F. Comparative competitive TAFC ELISA analysis of Protein A purified (2.5 µg mL^{-1}) and immunoaffinity purified (1 µg mL^{-1}) *anti*-TAFC IgG. Despite a lower concentration, the eluted antibody showed a significantly higher OD ($p < 0.0005$; unpaired *t*-test) than the Protein A-purified IgG. Flow-through from the immunoaffinity pull-down (F/T) showed no *anti*-TAFC activity confirming successful removal of *anti*-TAFC IgG.

the OD (450/620 nm) readings obtained from this screen for hybridomas that were ultimately selected and carried forward; named 1D1, 3B6, 3C7, and 6C6.

3.4. 6C6 hybridoma cell line produced anti-TAFC IgG

Protein A-purified IgG ($n = 2$) from hybridoma 6C6 (Supplementary Figs. 3A and B) was analysed to determine the optimal concentration of IgG for ELISA analysis whereby IgG (0.16–10 μg mL^{-1}) was added to ELISA plates coated with DAFC-BSA (0.12 μg mL^{-1}) (Fig. 4A) and revealed a concentration of 2.5 μg mL^{-1} for all further hybridoma-derived IgG ELISA analysis. To establish the extent of its specificity for TAFC, the IgG was screened by competitive TAFC ELISA using TAFC along with several other competitors (FsC, BmGT, ferrichrome, and ferri-ornibactin). The *anti*-TAFC IgG exhibited high specificity for $TAFC^{+Fe}$, showing competition, but not the other metabolites (Fig. 4B). Following assessment of the specificity of *anti*-TAFC IgG (Fig. 4B), it was apparent that the antibody was capable of detecting competitor $TAFC^{+Fe}$ concentrations lower than that previously tested. To assess this, a revised competitive TAFC ELISA was carried out with competing $TAFC^{+Fe}$ titred from 0.1 to 6.25 μM instead. This revised competitive TAFC ELISA analysis indicated the antibody was capable of detecting concentrations of $TAFC^{+Fe}$ as low as 0.1 μM (Fig. 4C). The IgG was also screened against *A. fumigatus* wild-type culture supernatant obtained following iron-free growth (which should contain TAFC), as a competitor. The fungal supernatant was ferrated in excess, quantified and added to the ELISA as a competitor alongside purified $TAFC^{+Fe}$. Anti-TAFC IgG showed similar competition for $TAFC^{+Fe}$ and ferrated wild-type supernatant at equivalent concentrations (Fig. 4C). However, as a limited supply of Protein A-purified *anti*-TAFC IgG from 6C6 culture (Fig. 4D) remained (slightly in excess of approximately 1200 μg), a strategy was proposed for the identification and expression of the *anti*-TAFC IgG (Fig. 1B).

3.5. Immunoaffinity purification of TAFC IgG

Protein A-purified *anti*-TAFC IgG was immunoaffinity purified using acetylated FsC-activated magnetic beads. Though 1200 μg of total putative TAFC-specific IgG was applied to the beads, and no TAFC-specific IgG appeared in the flow-through or wash, only 18 μg of TAFC–specific IgG (1.5% of total IgG applied) was eluted from the beads (Supplementary Figs. 4A and B; Supplementary Tables 1 and 2). Even considering incomplete elution of IgG from the beads, this amount was surprisingly low and suggests that the putative 6C6 hybridoma had been either (i) impure (i.e., contained multiple hybridomas) or (ii) a single or small number of hybridomas were secreting antibodies with multiple specificities, only one of which was TAFC-specific. In support of this, repeat antibody isotype analysis revealed the immunoaffinity-purified *anti*-TAFC IgG to actually be an IgG_{2a} (Fig. 4E), in contrast to initial analysis of the putative 6C6 hybridoma culture supernatant, which had indicted an IgG_3 isotype and supports the hypothesis that the *anti*-TAFC IgG comprised a sub-set of the total IgG produced by putative 6C6 hybridoma. Protein A-purified IgG (total IgG) (2.5 μg mL^{-1}), immunoaffinity-purified *anti*-TAFC IgG (1 μg mL^{-1}), and immunoaffinity beads flow-through (diluted to an equivalent of 2.5 μg mL^{-1} based on input) were analysed by competitive $TAFC^{+Fe}$ ELISA (Fig. 4F). The flow-through from immunoaffinity purification contained no *anti*-TAFC IgG activity indicating complete binding of all *anti*-TAFC IgG to the beads. The elution, though at a lower concentration than Protein A-purified IgG, resulted in a significantly higher OD than the Protein A purified IgG ($p < 0.0005$; unpaired *t*-test) in ELISA analysis. When converted to OD (450/620 nm) μg^{-1} protein input, Protein A-purified IgG had an absorbance of 0.23 OD μg^{-1} and immunoaffinity-purified IgG had an absorbance of 3.6 OD μg^{-1}, indicating a 15.6x functional enrichment. Protein A and immunoaffinity purified IgG were then analysed by SDS-PAGE (Fig. 4D). Two single bands corresponding to the heavy and light chains were observed for Protein A-purified IgG, while three bands corresponding to the heavy chain and two distinct light chains (light chains A and B; LCA and LCB) were observed for immunoaffinity-purified IgG. The bands associated with each were excised in three pieces and digested with trypsin, Asp-N, or Glu-C. Resultant peptides were analysed by LC-MS/MS with the aim of determining sufficient sequence information to allow recombinant antibody expression (Supplementary Tables 3–5).

3.6. LC-MS/MS analysis of affinity and immunoaffinity-purified TAFC IgG

Peptides associated with the heavy ($n = 1$) and light chain ($n = 2$) bands from SDS-PAGE LC-MS/MS analysis of immunoaffinity-purified *anti*-TAFC IgG were exported from PEAKS and assembled manually and using the ALPS assembler tool from [37]. For the heavy chain analysis, any peptides matching conserved IgG_3 domains were removed as they likely represented contaminating IgG_3 carried over from the Protein A-purified IgG during immunoaffinity purification. In several instances, two peptides were identified aligning to the same regions of the protein. Specifically, peptide conflicts were identified at predicted residue sites 4-23, 63-65, and 89-90. Using the different combinations this resulted in a total of 8 partial putative *anti*-TAFC IgG heavy chain sequences termed HC1.1–1.4 and HC2.1–2.4, these were grouped in naming HC1 or HC2 according to two conflicting sequences at the *N*-terminus (Supplementary Figs. 5A and 6A). As with the heavy chain, there were several instances where two peptides were identified aligning to the same regions of the protein for each of the two light chains. Specifically, at predicted residue sites 46-94 and 105-123 for light chain A, and residues 20-40 for light chain B. This resulted in a total of 4 possible *anti*-TAFC light chain sequences for light chain A and 2 possible sequences for light chain B (Supplementary Figs. 5B and 6B). Due to the conflicting peptide identifications, it was not possible to unequivocally determine the sequence of the full-length *anti*-TAFC antibody. However, it was possible to determine the sequences likely associated with the heavy and light chain *N*- and *C*-terminal regions based on the relative enrichment of peptides in the immunoaffinity-purified IgG. These in turn, were used to design degenerate primers to amplify the *anti*-TAFC IgG from 6C6 hybridoma cDNA (Supplementary Tables 4 and 5). However, it was not possible to unambiguously identify the κ light chain V_L-CH_1, by LC-MS/MS or targeted 6C6 hybridoma cDNA, and hence RNAseq of putative 6C6 hybridoma RNA was attempted.

3.7. RNA isolation and RNAseq analysis of 6C6 hybridoma RNA

Total RNA (192 μg; 55 μL @ 3.5 μg μL^{-1}) was isolated from the 6C6 hybridoma of which 47.95 μg was used for RNAseq analysis and yielded a total of 48,372,378 reads with an average read length of 100 bp and Q20(%) = 98.45% and % GC = 48.87%. Upon raw data receipt from BGI, 24 million paired-end reads were *de novo* assembled using Trinity v2.5.1 to yield a total 179,764 murine hybridoma-derived gene transcripts. We located Igh transcripts by determining if contigs contained 20–30-bp unique sequences of the Igh mouse constant region, these unique sequences have been used previously [41] to determine individual gene types (Ighg1:GGCCCCTGGATCTGCTGCCCAAA, Ighg2a:GTGTGTGGAGATACAACTGGCT, Ighg2b: CCAAAACAACACCCCCATCAG, Ighg2c:CCAAAACAACAGCCCCATCG, Ighg3:CTACAACAACAGCCCCATCTG). Similarly, Igl/Igk transcripts were located using the unique sequences of the mouse Igl/Igk constant regions (Igl1: GCCAGCCCAAGTCTTCGCCAT, Igl2: GTCAGCCCAAGTC CACTCCCACTC, Igl3: GTCAGCCCAAGTCCACTCCCACAC, Igl4: GCCAA CCCAAGGCTACACCCTCAG, Igk: GGGCTGATGCTGCACCAACTG). Ultimately, using the igfinder python script (http://tx.bioreg.kyushu-u.ac.jp/igfinder/) with a cutoff of 20–30 base pairs of unique sequences of the constant region and a length cutoff of >1200 and > 600 base pairs for heavy and light chains respectively, 43 nucleotide sequences of IgG

chains were identified.

3.8. Interrogation of antibody sequences from RNAseq analysis with mass spectra of anti-TAFC IgG before and after immunoaffinity purification

To determine the *anti*-TAFC IgG sequence, a proteo-transcriptomic strategy was implemented whereby RNAseq analysis of 6C6 hybridoma RNA was used in combination with LC-MS/MS analysis of the *anti*-TAFC IgG before and after immunoaffinity purification. Sequences from the RNAseq analysis (n = 43) were translated into the three possible reading frames and resultant peptide sequences were appended to the database for LC-MS/MS analysis. Mass spectra from the analysis of antibody heavy and light chains before and after *anti*-TAFC IgG immunoaffinity purification following in-gel (Fig. 4D) and in-solution digestion were then searched against this database using MaxQuant. Four of the identified protein groups contained leading proteins with RNAseq-derived sequences (Supplementary Table 6). Two of these included RNAseq derived heavy chain sequences; DN39396|c1|g13|i3195 was the only RNAseq-derived heavy chain protein exclusively detected after immunoaffinity purification (Supplementary Table 6). It was detected in peptides from band 3 that represented the heavy chain after immunoaffinity purification (Fig. 4D) as well as an in-solution digest of the entire *anti*-TAFC IgG after immunoaffinity purification (termed sample ID 6, relative to samples 1 to 5 in Fig. 4D). Two identified protein groups included RNAseq-derived light chain sequences. DN38318|c2|g2|i6177 was the only RNAseq derived light chain protein detected after immunoaffinity purification (Supplementary Table 6). Interestingly, it was also detected in the light chain band (Fig. 4D, band 2) before immunoaffinity purification and the heavy chain band after immunoaffinity purification (Fig. 4D, band 3). However, it was represented with the highest intensity and protein coverage in the light chain B band after immunoaffinity purification (Fig. 4D, band 5). Hence, the RNAseq-derived sequences DN39396|c1|g13|i3195 and DN38318|c2|g2|i6177 (Supplementary Figs. 6 and 7) were determined to correspond to the *anti*-TAFC IgG heavy and light chains respectively. The proposed sequences for the *anti*-TAFC IgG heavy and light chains are listed in Supplementary Table 7 along with their cognate DNA sequences from the RNAseq analysis. Both sequences were selected according to stop codons, but include additional *N*-termini sequences that were not predicted by MS and likely represents the signal peptides.

3.9. Final TAFC IgG heavy and light chain identification and CDR assignment

TAFC IgG heavy chain: V_H-CH_1 was assembled from protein LC-MS/MS, cDNA sequence and RNAseq analysis, allied to manual inspection of the data. Protein LC-MS/MS analysis provided sequence data for heavy chain CH_2–CH_3 assembly, allied to gap filling using RNAseq data (Supplementary Fig. 7B) and publicly available murine IgG_{2a} sequences. Although a signal peptide was identified for the heavy chain in the RNAseq analysis, a synthetic sequence was used for protein expression (Fig. 5A). Heavy chain CDR regions are shown in Fig. 5B. TAFC IgG light chain: V_L-C_L was assembled from protein LC-MS/MS and RNAseq analysis, allied to manual inspection of the data. Protein LC-MS/MS analysis of LCB provided sequence data for light chain C_L assembly, allied to gap filling using RNAseq data. Although a signal peptide was also identified for the light chain, an identical synthetic sequence to that deployed for heavy chain was deployed for protein expression (Fig. 5A). Light chain CDR regions are shown in Fig. 5B.

3.10. Recombinant antibody expression and specificity determination

Codon-optimised recombinant DNA for the full length heavy and light chain sequences shown in Fig. 5A was synthesised, cloned and transiently transfected into HEK293 for recombinant antibody expression by commercial arrangement. Recombinant antibody was successfully secreted, purified by Protein A affinity chromatography, and 5 mg IgG (0.3 mg mL^{-1}; 17 mL) was obtained and stored at −70 °C (Fig. 5C). Moreover, the single pot strategy for DAFC-BSA preparation proved successful as judged with recombinant TAFC immunoreactivity with resultant DAFC-BSA conjugates (Fig. 5D and E). Recombinant antibody was subsequently diluted to 1–2 ng mL^{-1} in 0.1% (w/v) BSA in TBST and

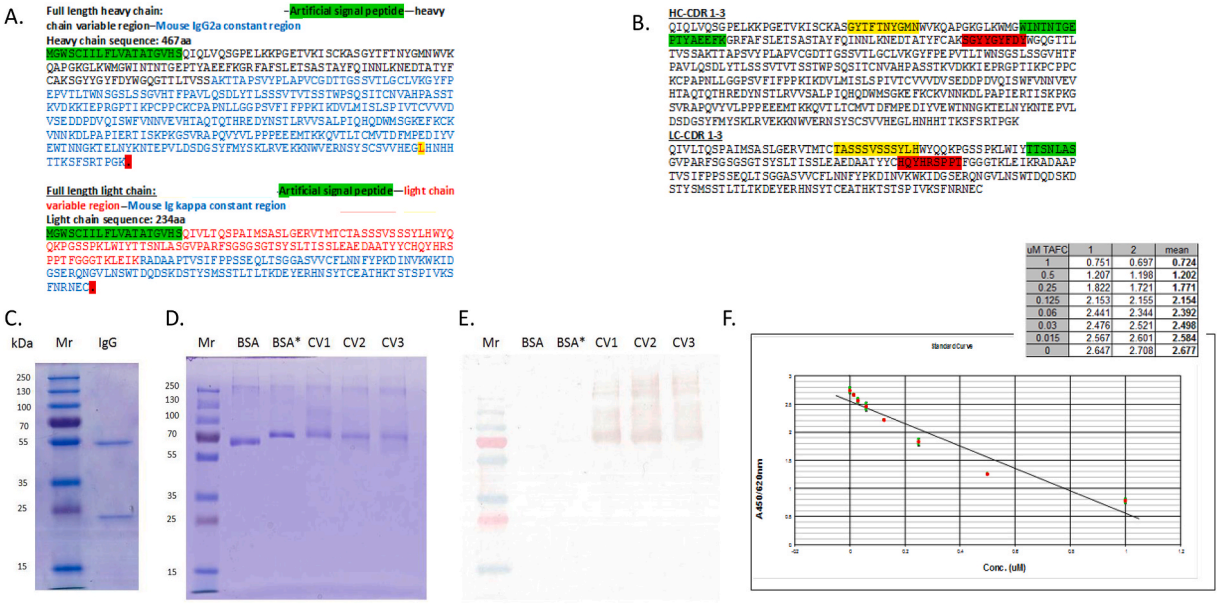

Fig. 5. A. Final TAFC IgG heavy and light chains sequences used for recombinant antibody expression [58–60]. B. Assignment of CDR regions in both HC and LC according to rules set out in http://www.bioinf.org.uk/abs/(Accessed 15 July 2018). CDR1: Yellow; CDR 2: Green and CDR3: Red in respective antibody chains. C. SDS-PAGE analysis of Recombinant IgG[*anti*-TAFC]; D. SDS-PAGE analysis of carrier protein (BSA), activated BSA (BSA*) and 3 batches of putative conjugate vaccines (CV1-3; 0.5 μg $track^{-1}$); E. Western blot analysis of carrier protein and conjugates, probed using recombinant IgG [TAFC] (@ 3 ng mL^{-1}), confirming TAFC conjugate vaccine synthesis. F. TAFC Competitive ELISA using recombinant TAFC IgG. (For interpretation of the references to colour in this figure legend, the reader is referred to the Web version of this article.)

screened for TAFC recognition by competitive ELISA (DAFC-BSA 0.12 μg mL^{-1} coating concentration) (Fig. 5F). The limit of detection was 15 nM $TAFC^{+Fe}$. A competitive LFT format was also developed using immobilised recombinant *anti*-TAFC IgG and DAFC-BSA sensitised AuNP, as schematically shown in Fig. 6A. Here, free $TAFC^{+Fe}$ competed with DAFC-BSA-AuNP for binding to immobilised *anti*-TAFC IgG during immunochromatography whereby increased amount of $TAFC^{+Fe}$ resulted in weaker line intensity. As shown in Fig. 6B, visible line formation, between DAFC-BSA-AuNP and immobilised *anti*-TAFC IgG, occurs in the absence of $TAFC^{+Fe}$ but is inhibited by greater than 3 ng $TAFC^{+Fe}$. This confirms detection of 3 ng $TAFC^{+Fe}$ in this novel immunoassay format. Moreover, an alternative format involving membrane- and AuNP-immobilised DAFC-BSA, respectively, plus solution-phase *anti*-TAFC IgG, was also developed. Surprisingly, free $TAFC^{+Fe}$ also inhibited line formation in this system, which infers a binding stoichiometry of 2 mol $TAFC^{+Fe}$ *anti*-TAFC IgG^{-1} (Fig. 6C).

4. Discussion

Current *in vitro* diagnostic methods utilised for IPA suffer from shortcomings such as the possible detection of other mycoses. In contrast, detecting specific siderophores can provide precise information on infecting species. For example, TAFC is only produced by *Aspergillus, Fusarium,* and *Nectria* species [19]. Although TAFC detection has been proposed as a urinary biomarker for the diagnosis of IPA, no facile method is available for analyte detection. Here we demonstrate, for the first time, that acetylated FsC^{+Fe} can be conjugated to KLH using SMCC/SATA chemistry. The resultant siderophore-protein conjugate was immunogenic in mice and facilitated generation of a TAFC-specific antibody. Due to hybridoma instability and impurity issues, it proved essential to ultimately sequence the TAFC-specific mAb heavy and light chains using a combined proteo-transcriptomic approach. It is widely acknowledged that mAbs produced in cultured hybridoma cell lines can be unstable. Sequencing of mAb variable regions is hence critical in preserving mAb characteristics and overcoming challenges such as IgG rearrangements and impacts of hybridoma cell loss and hybridoma instability caused by mutations, chromosome deletions, or environmental factors [33,43]. Sequencing of the *anti*-TAFC IgG enabled CDR identification and subsequent recombinant expression of the TAFC-specific IgG_{2a} mAb (5 mg) in HEK293 cells. The resultant recombinant antibody was then used to develop a TAFC-specific ELISA (detection limit: 6 ng mL^{-1}) and a LFT for TAFC detection. Moreover, the antibody was also used to confirm that a single-tube reaction allowed FsC^{+Fe} acetylation, activation via SMCC and conjugation to SATA-modified BSA ($n = 3$) in a facile manner which infers the potential of a conjugate vaccine to attenuate TAFC-mediated iron uptake by *A. fumigatus* in infected individuals.

$TAFC^{+Fe}$ possesses limited functional groups for standard crosslinker modification, so an analog strategy was used to develop the TAFC immunogen. Conjugation of the siderophore analog, acetylated FsC^{+Fe}, to the carrier protein, KLH, was mediated by heterobifunctional crosslinkers, sulpho-SMCC and SATA, respectively [29,30]. Thus, by acetylating two amine groups on FsC^{+Fe} using SNA, to generate DAFC, the third amine group remained available for further NHS ester modification, whereby acetylated FsC^{+Fe} was conjugated to the carrier protein, KLH. Importantly, TAFC generated by SNA acetylation shared an LC-MS/MS retention time and fragmentation pattern with that of native TAFC acetylated by the *A. fumigatus* acetyltransferase, SidG. Furthermore, uptake of fluorescently labelled DAFC by *A. fumigatus* has recently been demonstrated [44]. FsC^{+Fe} acetylated with limiting SNA actually generated a heterogeneous mixture of FsC, MAFC, DAFC, and TAFC (collectively termed acetylated FsC^{+Fe}). It was decided to not RP-HPLC purify any acetylated form of FsC^{+Fe} from this reaction mixture and to generate a heterogeneous immunogen predominantly containing MAFC-KLH and DAFC-KLH. Following hybridoma development, $TAFC^{+Fe}$-specific antibody was ultimately selected by competitive ELISA in the presence of $TAFC^{+Fe}$ only.

A strategy for TAFC conjugation to proteins was suggested, although it was not reduced to practice [45]. We previously attempted TAFC conjugation to carrier proteins, via a photochemical approach, and although indicative seroreactivity was subsequently observed to protein-conjugated TAFC, it proved impossible to unambiguously confirm reactivity towards free TAFC. Carroll et al. undertook base hydrolysis of coprogen to produce dimerum acid and *N*-acetyl fusarinine followed by conjugation to BSA for use as antigens for mAb production [46]. Although seroreactivity was observed against hydrolysed coprogen and TAFC in bleeds from immunised animals, no production of a TAFC-specific mAb was evident. Overall, this underlines the extreme technical difficulty associated with TAFC conjugation to proteins. The strategy presented herein which involved production of an activated

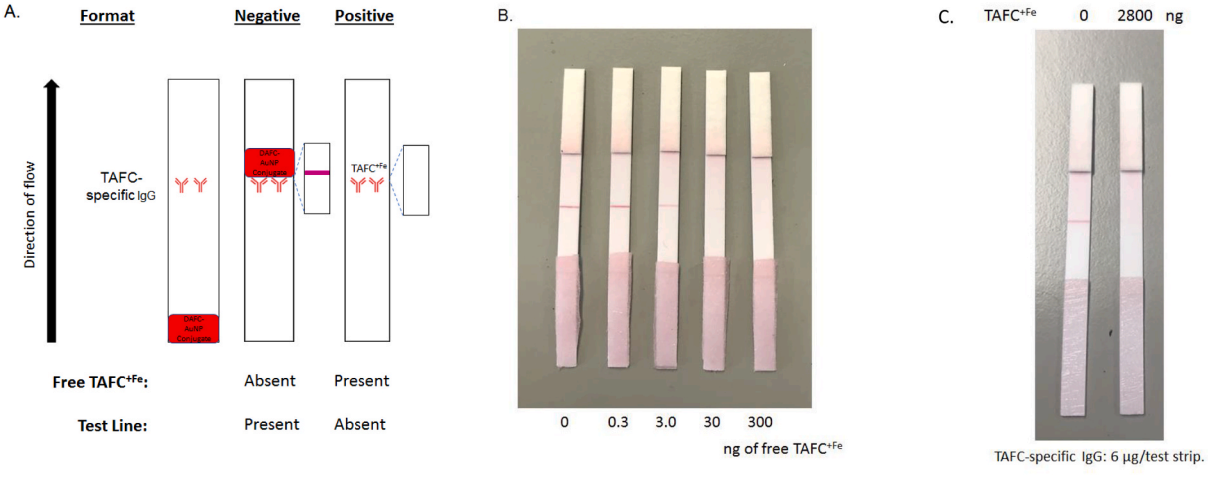

Fig. 6. A. Schematic assay format for TAFC detection by lateral flow test (LFT) technology. Prior to assay, TAFC-specific IgG was sprayed on nitrocellulose membranes and DAFC-BSA was conjugated to gold nanoparticles (DAFC-BSA-AuNP). In the absence of free $TAFC^{+Fe}$, the DAFC-BSA-AuNP conjugate is immobilised on the membrane generating a visible line. In the presence of $TAFC^{+Fe}$, DAFC-BSA-AuNP immobilisation is inhibited as the amount of free $TAFC^{+Fe}$ increases. At high $TAFC^{+Fe}$ no line is visible. B. Free $TAFC^{+Fe}$ (3 ng) begins to inhibit signal generation in the LFT which is completely inhibited at 300 ng. C. An alternative LFT format comprising membrane immobilised DAFC-BSA and AuNP-conjugated DAFC-BSA, along with free TAFC-specific IgG. Free $TAFC^{+Fe}$ prevents line formation indicating binding stoichiometry of 2 mol $TAFC^{+Fe}$ mol IgG^{-1}. (For interpretation of the references to colour in this figure legend, the reader is referred to the Web version of this article.)

TAFC-analog, DAFC, followed by conjugation to a carrier protein resulted in immunogen synthesis, as confirmed siderophore presence (A440nm) in immunogen preparations following dialysis. This 'TAFC analog strategy' which then enabled TAFC-specific antibody generation, overcame the difficulties associated with all previous attempts at generating TAFC-specific antisera. Moreover, the antibodies raised in mice recognised DAFC-conjugated to an unrelated protein (i.e., BSA) and free $TAFC^{+Fe}$ specifically inhibited antibody binding to protein-conjugated DAFC. Related and unrelated *A. fumigatus* and bacterial siderophores/metabolites (i.e., FsC, ornibactin, BmGT or ferrichrome) did not inhibit binding indicating the antibody was capable of recognising $TAFC^{+Fe}$ with a high degree of specificity. It was therefore unfortunate that although stable hybridoma generation initially appeared successful, that for unknown reasons instability occurred resulting in a limited availability of putative TAFC-specific mAb.

The preparation of DAFC-conjugated paramagnetic beads facilitated immunoaffinity purification of TAFC-specific mAb (18 μg) and LC-MS/MS, allied to Isostrip™ analysis, confirmed that this was an IgG_{2a}. This contrasted with analysis of the antibody prior to immunoaffinity purification, which indicated an IgG_3 isotype, and suggested the hybridoma population contained single or multiple hybridomas secreting different antibodies. The issue of lack of monoclonality is widespread and it has been estimated that upwards of 30% of 'monoclonal' antibody preparations are impure with expression of multiple functional heavy and light chains [47]. It has also been reported that some SP2/O cell lines used for cell fusion secrete non-specific Igs which can potentially represent contaminating transcripts when determining VR heavy and light chains [48]. Though it proved possible to assemble the majority of the heavy chain sequence from gel LC-MS/MS analysis of immunoaffinity purified *anti*-TAFC IgG following the ALPS pipeline [37], determination of CDR regions in the heavy and light chains proved impossible. This was ultimately resolved by complementary cDNA sequence analysis and RNAseq of total hybridoma RNA which allowed assembly of putative TAFC IgG-specific heavy and light chain sequences by combinatorial, iterative and manual inspection of all data sources. High throughput sequencing platforms have been used previously to successfully sequence antibody variable domains [41,49,50]. Although the native signal sequences for the heavy and light chains were identified (Supplementary Table 7), it was decided to use a signal sequence proposed by the commercial provider to facilitate IgG secretion in mammalian cell culture system.

After sequence determination the full-length *anti*-TAFC IgG was recombinantly expressed in HEK293 cells. The recombinant antibody was first used to confirm the single pot approach for DAFC-BSA synthesis, the significance of which is that DAFC-protein immunogens can be readily synthesised for both immunoassay, and future immunogen use for animal or human vaccination studies. For instance, substitution of BSA with Cross-Reacting Material 197 (CRM197) [51], the latter an established vaccine carrier protein, could facilitate siderophore-protein conjugate synthesis for the development of human anti-Aspergillus vaccines [52,53]. Competitive ELISA analysis indicated the recombinant *anti*-TAFC antibody was highly sensitive and could detect $TAFC^{+Fe}$ at as low as 15 nM (Fig. 5F). LFT analysis indicated a sensitivity of detection of 3 ng $TAFC^{+Fe}$ (Fig. 6A and B). Early stage sample analysis of the levels of TAFC in the sera of patients with suspected or probable/proven Aspergillosis detected mean values of 11.6 ng mL^{-1} (13 nM) and 9.7 ng mL^{-1} (11 nM), respectively [25]. Further, analysis of TAFC levels in urine from a rat model of Aspergillosis indicated a mean value of 370 ng mL^{-1} (408.5 nM) [26]. The recombinant *anti*-TAFC IgG is therefore within the range of clinically relevant levels for the detection of Aspergillosis. Hence, this antibody has the functional utility for implementation in an *in vitro* diagnostic assay. The competitive $TAFC^{+Fe}$ –specific LFT has significant potential as a facile method for urinary siderophore detection, and subject to further development, for deployment as a useful point-of-care (POC) diagnostic for IPA. Indeed, the availability of POC assays has been highlighted as complementary technologies such as LFTs and image analysers are merged to improve infectious disease diagnosis and patient care [54]. To our knowledge, there is no description of a lateral flow test with equivalent sensitivity for siderophore detection in the literature, even though alternative technologies such as Raman spectroscopy have been explored for rapid siderophore detection [55]. Undoubtedly, given the development of immunoassays to detect Mycobacterial macrolide cytotoxins and siderophores like mycolactones and carboxybactin, respectively [56,57] we are undoubtedly entering a new era of small molecule detection to enable reliable diagnosis of refractory infectious diseases. As previously discussed, chelation of TAFC to gallium (^{68}Ga) as opposed to iron generates an effective tool for positron-emission tomography (PET)-based imaging. The $TAFC^{+Fe}$-specific mAb presented herein may also find application in the detection and quantification of ^{68}Ga-TAFC for regulatory and research purposes.

5. Conclusions

In conclusion, we have generated a recombinant TAFC-specific mAb, developed facile conjugate immunogen strategies and formulated two TAFC-specific detection systems (ELISA and LFT). In combination, these advances readily enable the development of TAFC-detection systems for clinical use, and potentially the immunotherapeutic use of TAFC immunogens to prevent or ameliorate IPA.

CRediT authorship contribution statement

Nicola M. Moloney: compiled and wrote the manuscript, performed experimentation. **Annemarie Larkin:** performed experimentation. **Linan Xu:** performed experimentation. **David A. Fitzpatrick:** compiled and wrote the manuscript, performed experimentation. **Holly L. Crean:** performed experimentation. **Kieran Walshe:** performed experimentation. **Hubertus Haas:** contributed reagents, aided data interpretation and provided intellectual input. **Clemens Decristoforo:** contributed reagents, aided data interpretation and provided intellectual input. **Sean Doyle:** performed experimentation, compiled and wrote the manuscript, is corresponding author, All authors edited and approved the submitted manuscript version.

Acknowledgements

This work was funded by a Science Foundation Ireland Investigator Award to SD (12/IP/1695). Quantitative mass spectrometry facilities were funded by a competitive infrastructure award from Science Foundation Ireland (12/RI/2346(3)). We acknowledge Caroline Batchelor (Department of Biology, Maynooth University) for extensive support and maintenance of LC-MS facilities and Nicholas Irani (Department of Biology, Maynooth University) for maintenance of the RP-HPLC systems. We also acknowledge Dr Andrew McCann (National Institute for Cellular Biotechnology, Dublin City University) for his training on hybridoma development. The authors would also like to gratefully acknowledge the technical staff of the RCSI Biomedical Research Facility, Beaumont Hospital, Dublin, Ireland.

Appendix A. Supplementary data

Supplementary data to this article can be found online at https://doi.org/10.1016/j.ab.2021.114384.

References

[1] K.M. Pianalto, J.A. Alspaugh, in: Maurizio Del Poeta (Ed.), New Horizons in Antifungal Therapy, 4th, 2, J Fungi, Basel, 2016, pp. 1–26, https://doi.org/10.3390/jof2040026.

[2] F. Bongomin, S. Gago, R.O. Oladele, D.W. Denning, Global and Multi-National Prevalence of Fungal Diseases-Estimate Precision 4(57), 3, J. Fungi, 2017, 10.3390/jof3040057.

[3] T.R. Dagenais, N.P. Keller, Pathogenesis of Aspergillus fumigatus in invasive aspergillosis, Clin. Microbiol. Rev. 22 (2009) 447–465.

[4] J.P. Latgé, G. Chamilos, Aspergillus fumigatus and aspergillosis in 2019, Clin. Microbiol. Rev. 33 (1) (2019) e00140–18, https://doi.org/10.1128/CMR.00140-18.

[5] A. Abad, J.V. Fernández-Molina, J. Bikandi, A. Ramírez, J. Margareto, J. Sendino, F.L. Hernando, J. Pontón, J. Garaizar, A. Rementeria, What makes Aspergillus fumigatus a successful pathogen? Genes and molecules involved in invasive aspergillosis, Rev. Iberoam. De. Micol. 27 (2010) 155–182.

[6] K.J. Kwon-Chung, J.A. Sugui, What do we know about the role of gliotoxin in the pathobiology of Aspergillus fumigatus? Med. Mycol. 47 (Suppl 1) (2009) S97–S103.

[7] A. Margalit, K. Kavanagh, The innate immune response to Aspergillus fumigatus at the alveolar surface, FEMS Microbiol. Rev. 39 (2015) 670–687.

[8] B.H. Segal, R. Herbrecht, D.A. Stevens, L. Ostrosky-Zeichner, J. Sobel, C. Viscoli, T. J. Walsh, J. Maertens, T.F. Patterson, J.R. Perfect, B. Dupont, J.R. Wingard, T. Calandra, C.A. Kauffman, J.R. Graybill, L.R. Baden, P.G. Pappas, J.E. Bennett, D. P. Kontoyiannis, C. Cordonnier, M.A. Viviani, J. Bille, N.G. Almyroudis, L.J. Wheat, W. Graninger, E.J. Bow, S.M. Holland, B.J. Kullberg, W.E. Dismukes, B.E. De Pauw, Defining responses to therapy and study outcomes in clinical trials of invasive fungal diseases: mycoses Study Group and European Organization for Research and Treatment of Cancer consensus criteria, Clin. Infect. Dis. 47 (2008) 674–683.

[9] R.C. Barton, Laboratory diagnosis of invasive aspergillosis: from diagnosis to prediction of outcome, Sci. Tech. Rep. 2013 (2013) 459405.

[10] N.A.R. Gow, J.P. Latge, C.A. Munro, The fungal cell wall: structure, biosynthesis, and function, Microbiol. Spectr. 5 (2017).

[11] G. Johnson, A. Ferrini, S.K. Dolan, T. Nolan, S. Agrawal, S. Doyle, S.A. Bustin, Biomarkers for invasive aspergillosis: the challenges continue, Biomarkers Med. 8 (2014) 429–451.

[12] V.B. Krylov, A.S. Solovev, D.A. Argunov, J.P. Latge, N.E. Nifantiev, Reinvestigation of carbohydrate specificity of EB-A2 monoclonal antibody used in the immune detection of Aspergillus fumigatus galactomannan, Heliyon 5 (2019), e01173.

[13] M. Hoenigl, S. Eigl, S. Heldt, W. Duettmann, C. Thornton, J. Prattes, Clinical evaluation of the newly formatted lateral-flow device for invasive pulmonary aspergillosis, Mycoses 61 (2018) 40–43.

[14] K. Reiber, E.P. Reeves, C.M. Neville, R. Winkler, P. Gebhardt, K. Kavanagh, S. Doyle, The expression of selected non-ribosomal peptide synthetases in Aspergillus fumigatus is controlled by the availability of free iron, FEMS (Fed. Eur. Microbiol. Soc.) Microbiol. Lett. 248 (2005) 83–91.

[15] M. Schrettl, E. Bignell, C. Kragl, C. Joechl, T. Rogers, H.N. Arst, K. Haynes, H. Haas, Siderophore biosynthesis but not reductive iron assimilation is essential for Aspergillus fumigatus virulence, J. Exp. Med. 200 (2004) 1213–1219.

[16] A.H. Hissen, A.N. Wan, M.L. Warwas, L.J. Pinto, M.M. Moore, The Aspergillus fumigatus siderophore biosynthetic gene sidA, encoding L-ornithine N5-oxygenase, is required for virulence, Infect. Immun. 73 (2005) 5493–5503.

[17] M. Petrik, H. Haas, G. Dobrozemsky, C. Lass-Flörl, A. Helbok, M. Blatzer, H. Dietrich, C. Decristoforo, 68Ga-siderophores for PET imaging of invasive pulmonary aspergillosis: proof of principle, J. Nucl. Med. 51 (2010) 639–645.

[18] M. Schrettl, E. Bignell, C. Kragl, Y. Sabiha, O. Loss, M. Eisendle, A. Wallner, H. N. Arst Jr., K. Haynes, H. Haas, Distinct roles for intra- and extracellular siderophores during Aspergillus fumigatus infection, PLoS Pathog. 3 (2007) 1195–1207.

[19] H. Haas, Fungal siderophore metabolism with a focus on Aspergillus fumigatus, Nat. Prod. Rep. 31 (2014) 1266–1276.

[20] M.T. Martínez-Pastor, S. Puig, Adaptation to iron deficiency in human pathogenic fungi, Biochim Biophys Acta Mol Cell Res, 2020, p. 118797.

[21] H. Haas, M. Petrik, C. Decristoforo, An iron-mimicking, Trojan horse-entering fungi–has the time come for molecular imaging of fungal infections? PLoS Pathog. 11 (2015), e1004568.

[22] M. Petrik, H. Haas, M. Schrettl, A. Helbok, M. Blatzer, C. Decristoforo, In vitro and in vivo evaluation of selected 68Ga-siderophores for infection imaging, Nucl. Med. Biol. 39 (2012) 361–369.

[23] M. Petrik, C. Zhai, H. Haas, C. Decristoforo, Siderophores for molecular imaging applications, Clin Transl Imaging 5 (2017) 15–27.

[24] J.M. Doyle, K. Walshe, N. Gordon, K. Kavanagh, L. Gallagher, Method for Detecting Infections, 2018. EP 2709659.

[25] C.S. Carroll, L.N. Amankwa, L.J. Pinto, J.D. Fuller, M.M. Moore, Detection of a serum siderophore by LC-MS/MS as a potential biomarker of invasive aspergillosis, PloS One 11 (2016), e0151260.

[26] D. Luptáková, T. Pluháček, M. Petřík, J. Novák, A. Palyzová, L. Sokolová, A. Škríba, B. Šedivá, K. Lemr, V. Havlíček, Non-invasive and invasive diagnoses of aspergillosis in a rat model by mass spectrometry, Sci. Rep. 7 (2017) 16523.

[27] M. Hoenigl, T. Orasch, K. Faserl, J. Prattes, J. Loeffler, J. Springer, F. Gsaller, F. Reischies, W. Duettmann, R.B. Raggam, H. Lindner, H. Haas, C. Triacetylfusarinine, A urine biomarker for diagnosis of invasive aspergillosis, J. Infect. 78 (2019) 150–157.

[28] T. Orasch, J. Prattes, K. Faserl, S. Eigl, W. Düttmann, H. Lindner, H. Haas, M. Hoenigl, Bronchoalveolar lavage triacetylfusarinine C (TAFC) determination for diagnosis of invasive pulmonary aspergillosis in patients with hematological malignancies, J. Infect. 75 (2017) 370–373.

[29] M. Fox, G. Gray, K. Kavanagh, C. Lewis, S. Doyle, Detection of Aspergillus fumigatus mycotoxins: immunogen synthesis and immunoassay development, J. Microbiol. Methods 56 (2004) 221–230.

[30] N.M. Moloney, R.A. Owens, P. Meleady, M. Henry, S.K. Dolan, E. Mulvihill, M. Clynes, S. Doyle, The iron-responsive microsomal proteome of Aspergillus fumigatus, Journal of Proteomics 136 (2016) 99–111.

[31] D. O'Sullivan, M. Henry, H. Joyce, N. Walsh, E. Mc Auley, P. Dowling, N. Swan, M. Moriarty, P. Barnham, M. Clynes, A. Larkin, 7B7: a novel antibody directed against the Ku70/Ku80 heterodimer blocks invasion in pancreatic and lung cancer cells, Tumour Biol 35 (2014) 6983–6997.

[32] S.K. Dolan, R.A. Owens, G. O'Keeffe, S. Hammel, D.A. Fitzpatrick, G.W. Jones, S. Doyle, Regulation of nonribosomal peptide synthesis: bis-thiomethylation attenuates gliotoxin biosynthesis in Aspergillus fumigatus, Chem. Biol. 21 (2014) 999–1012.

[33] G. Köhler, C. Milstein, Continuous cultures of fused cells secreting antibody of predefined specificity, Nature 256 (1975) 495–497.

[34] A. Shevchenko, H. Tomas, J. Havlis, J.V. Olsen, M. Mann, In-gel digestion for mass spectrometric characterization of proteins and proteomes, Nat. Protoc. 1 (2006) 2856–2860.

[35] G. O'Keeffe, S. Hammel, R.A. Owens, T.M. Keane, D.A. Fitzpatrick, G.W. Jones, S. Doyle, RNA-seq reveals the pan-transcriptomic impact of attenuating the gliotoxin self-protection mechanism in Aspergillus fumigatus, BMC Genom. 15 (894) (2014), https://doi.org/10.1186/1471-2164-15-894.

[36] R.A. Owens, G. O'keeffe, E.B. Smith, S.K. Dolan, S. Hammel, K.J. Sheridan, D. A. Fitzpatrick, T.M. Keane, G.W. Jones, S. Doyle, Interplay between gliotoxin resistance, secretion, and the methyl/methionine cycle in Aspergillus Fumigatus, Eukaryot. Cell 14 (2015) 941–957.

[37] N.H. Tran, M.Z. Rahman, L. He, L. Xin, B. Shan, M. Li, Complete de novo assembly of monoclonal antibody sequences, Sci. Rep. 6 (2016) 31730.

[38] M.B. Swindells, C.T. Porter, M. Couch, J. Hurst, K.R. Abhinandan, J.H. Nielsen, G. Macindoe, J. Hetherington, A.C. Martin, abYsis: integrated antibody sequence and structure-management, analysis, and prediction, J. Mol. Biol. 429 (2017) 356–364.

[39] A.M. Bolger, M. Lohse, B. Usadel, Trimmomatic: a flexible trimmer for Illumina sequence data, Bioinformatics 30 (2014) 2114–2120.

[40] M.G. Grabherr, B.J. Haas, M. Yassour, J.Z. Levin, D.A. Thompson, I. Amit, X. Adiconis, L. Fan, R. Raychowdhury, Q. Zeng, Z. Chen, E. Mauceli, N. Hacohen, A. Gnirke, N. Rhind, F. di Palma, B.W. Birren, C. Nusbaum, K. Lindblad-Toh, N. Friedman, A. Regev, Full-length transcriptome assembly from RNA-Seq data without a reference genome, Nat. Biotechnol. 29 (2011) 644–652.

[41] Y. Kuniyoshi, K. Maehara, T. Iwasaki, M. Hayashi, Y. Semba, M. Fujita, Y. Sato, H. Kimura, A. Harada, Y. Ohkawa, Identification of immunoglobulin gene sequences from a small read number of mRNA-seq using hybridomas, PloS One 11 (2016), e0165473.

[42] P. Stothard, The sequence manipulation suite: JavaScript programs for analyzing and formatting protein and DNA sequences, Biotechniques 28 (2000) 1102–1104.

[43] J.M. Coco-Martin, J.W. Oberink, T.A.M. van der Velden-de Groot, E.C. Beuvery, Methods for studying the stability of antibody expression by hybridoma cells in homogeneous continuous culture systems, Anal. Chim. Acta 249 (1991) 257–262.

[44] J. Pfister, A. Lichius, D. Summer, H. Haas, T. Kanagasundaram, K. Kopka, C. Decristoforo, Live-cell imaging with Aspergillus fumigatus-specific fluorescent siderophore conjugates, Sci. Rep. 10 (2020) 15519.

[45] M. Moore Margo, A.H.T. Hissen, N.C.A. Wan, Production of Mutant Strain of *Aspergillus fumigatus*, Method of Assay for Inhibiting Siderophore Biosynthesis and Diagnostic Method for Detecting Likely *Aspergillus fumigatus* Infection, US Patent US7794712B2, 2004.

[46] C. Carroll, L.J.S. Pinto, M.M. Moore, The importance of secreted siderophores in the diagnosis of invasive aspergillosis, in: 5th Advances against Aspergillosis Meeting. Abstract 130, Advances Against Aspergillosis, 2012, 201–201, http://www.advancesagainstaspergillosis.org/2016/AAA2012Abstract%20Book_Final.pdf.

[47] A.R.M. Bradbury, N.D. Trinklein, H. Thie, I.C. Wilkinson, A.K. Tandon, S. Anderson, C.L. Bladen, B. Jones, S.F. Aldred, M. Bestagno, O. Burrone, J. Maynard, F. Ferrara, J.S. Trimmer, J. Görnemann, J. Glanville, P. Wolf, A. Frenzel, J. Wong, X.Y. Koh, H.Y. Eng, D. Lane, M.P. Lefranc, M. Clark, S. Dübel, When monoclonal antibodies are not monospecific: hybridomas frequently express additional functional variable regions, mAbs 10 (2018) 539–546.

[48] L. Babrak, J.A. McGarvey, L.H. Stanker, R. Hnasko, Identification and verification of hybridoma-derived monoclonal antibody variable region sequences using recombinant DNA technology and mass spectrometry, Mol. Immunol. 90 (2017) 287–294.

[49] M. Schanz, T. Liechti, O. Zagordi, E. Miho, S.T. Reddy, H.F. Günthard, A. Trkola, M. Huber, High-throughput sequencing of human immunoglobulin variable regions with subtype identification, PloS One 9 (2014), e111726.

[50] K.A. Henry, Next-generation DNA sequencing of V(H)/V(L) repertoires: a primer and guide to applications in single-domain antibody discovery, Methods Mol. Biol. 1701 (2018) 425–446.

[51] T.E. MacCalman, M.K. Phillips-Jones, S.E. Harding, Glycoconjugate vaccines: some observations on carrier and production methods, Biotechnol. Genet. Eng. Rev. 35 (2019) 93–125.

[52] S.M. Levitz, Aspergillus vaccines: hardly worth studying or worthy of hard study? Med. Mycol. 55 (2017) 103–108.

[53] L.A. Mike, S.N. Smith, C.A. Sumner, K.A. Eaton, H.L. Mobley, Siderophore vaccine conjugates protect against uropathogenic Escherichia coli urinary tract infection, Proc. Natl. Acad. Sci. U. S. A. 113 (2016) 13468–13473.

[54] J.D. Jenks, M. Hoenigl, Point-of-care diagnostics for invasive aspergillosis: nearing the finish line, Expert Rev. Mol. Diagn (2020) 1–9.

[55] S. Pahlow, T. Orasch, O. Žukovskaja, T. Bocklitz, H. Haas, K. Weber, Rapid detection of the aspergillosis biomarker triacetylfusarinine C using interference-enhanced Raman spectroscopy, Anal. Bioanal. Chem. 412 (2020) 6351–6360.

[56] R. McNerney, M. Moyo, A novel small molecule immunoassay to detect the mycobacterial siderophore carboxymycobactin, Biomedical and Biotechnology Research Journal (BBRJ) 1 (2017) 37–41.
[57] L. Warryn, J.P. Dangy, P. Gersbach, M. Gehringer, A. Schäfer, M.T. Ruf, N. Ruggli, K.H. Altmann, G. Pluschke, Development of an ELISA for the quantification of mycolactone, the cytotoxic macrolide toxin of Mycobacterium ulcerans, PLoS Negl Trop Dis 14 (2020), e0008357.
[58] F. Sievers, A. Wilm, D. Dineen, T.J. Gibson, K. Karplus, W. Li, R. Lopez, H. McWilliam, M. Remmert, J. Söding, J.D. Thompson, D.G. Higgins, Fast, scalable generation of high-quality protein multiple sequence alignments using Clustal Omega, Mol. Syst. Biol. 7 (2011) 539.
[59] R.C. Edgar Muscle, Multiple sequence alignment with high accuracy and high throughput, Nucleic Acids Res. 32 (2004) 1792–1797.
[60] A. Guthals, Y. Gan, L. Murray, Y. Chen, J. Stinson, G. Nakamura, J.R. Lill, W. Sandoval, N. Bandeira, De novo MS/MS sequencing of native human antibodies, J. Proteome Res. 16 (2017) 45–54.